Colloid Journal, Vol. 66, No. 1, 2004, pp. 84–94. Translated from Kolloidnyi Zhurnal, Vol. 66, No. 1, 2004, pp. 95–107.

Interactions between Langmuir–Blodgett Polymer Monolayers Studied with the Surface Force Apparatus

L. A. Tsarkova[1, 2], P. V. Protsenko[1, 2], and J. Klein[1, 3]

[1] *Weizmann Institute of Science, Rehovot, 76100, Israel*
[2] *Department of Chemistry, Moscow State University, Vorob'evy gory, Moscow, 119899 Russia*
[3] *Physical and Theoretical Chemistry Laboratory, Oxford OX1 3QZ, UK*

Received February 7, 2003

Abstract—Langmuir–Blodgett monolayers from end-functionalized polyisoprene (PI–X) were studied in a surface force apparatus (SFA) as a model of a highly stretched brush melt. After deposition on a freshly cleaved mica, two identical brush monolayers (with surface area per molecule of about 170 Å^2) were brought into adhesive contact in the SFA; then kinetic changes in the film thickness and the topography of the contact were continuously monitored. We observed spontaneous thinning of the brush melt bilayer. This effect can be attributed to the enhanced lateral motion of the sticking end-groups under the "contact induced pressure." The possible model describing kinetic changes in the film thickness is presented. The behavior of the two opposing brush melts and a single brush monolayer in contact with two mica surfaces was compared. Molecular mechanisms involved in the rearrangements of brush melts are proposed for both systems.

1. INTRODUCTION

End-functionalized polymers are a class of amphiphylic molecules in which the ionic or zwitterionic group at the end of the polymer chain represents the hydrophilic part, and the hydrophobic part is usually an oil-soluble macromolecule. Such polymers can be considered as structural analogs of regular surfactants and indeed they have a number of properties in common with low-molecular-weight surfactants. Thus, dynamic light scattering measurements showed that, in dilute solutions of end-functionilised polyisoprenes, molecular aggregates are formed and the critical association concentration of such polymer micelles is determined by the concentration of polar end groups [1].

Another similarity to the regular surfactant's behavior is that, in a good solvent, end-functionalized polymers adsorb on a solid surface via the end group. As a result, a "swollen polymer brushes" are formed, which strongly modify interfacial properties. In this case the lateral spacing s between the grafted ends is considerably lower than the dimensions of the undisturbed polymer coil (Fig. 1a). The brush height h is determined by the balance between the osmotic interactions tending to stretch the molecules normal to the surface and the decrease in entropy due to the stretching [2–4].

Compared to the adsorbed layers of low-molecular-weight surfactants, polymer brushes have a number of advantages determined by the long polymeric tail, such as much more extended adsorbed layers, higher mechanical stability of the adsorbed layer and better lubricating properties. This explains immense practical and fundamental interest in such brushes, especially in the steric stabilization of colloids [5, 6], regulation of surfaces wettability [7] and lubrication [8, 9].

The case of interactions between densely attached, solvent-free polymer melt brushes (Fig. 1b) is of considerable interest. Such systems have been relatively neglected in comparison with the swollen brushes. The specific highly stretched configuration of the polymer chains in a molten brush implies different behavior than in usual polymer films. However, there have been so far only few experimental publications on the characterization and properties of the monodispersed molten brushes. This is explained by experimental difficulties to achieve high grafting conditions, which are usually assumed in theories. Physical adsorption from the solution of end-terminated polymers is too weak to provide a high grafting density. As a result, very thin (or even noncontinuous) polymer layer is left on a substrate upon the removal of a solvent.

A more controllable brush layer can be obtained by the chemical grafting of the chain ends [10, 11] or by the adsorption of a diblock copolymers on the surface [12] resulting in a segregated lamella phase (Fig. 1c). Though even in these cases, usually only a limited surface coverage can be achieved. Additionally, it is difficult to apply chemical grafting procedure to the inert mica surface, which is conveniently used in the surface force apparatus (SFA) for measuring surface separations with several angstroms resolution due to atomically smooth surface (see experimental section).

An interesting approach to create surface layers of polymer melt brushes on solid substrates is to utilize the ability of end-functionalized polymers to form stable Langmuir monolayers on water surface, which can be than transferred onto solid substrates via the

1061-933X/04/6601-0084 © 2004 MAIK "Nauka / Interperiodica"

Blodgett technique. Recently, a highly stretched brush melt monolayers of polyisoprenes have been described [13, 14]. The compression isotherms are dominated by the entropy change due to the stretching of polymer chains upon lateral compression [14]. The thickness of the monolayers at the air/water interface has been characterized by X-ray reflectivity measurements and was shown to be inversely proportional to the area per head group in accordance with a model assuming a solvent-free hydrophobic layer of the same density as the bulk material. When transferred onto solid substrates, these monolayers can be regarded as dense incompressible brush melts with controllable grafting density and thickness, and can be directly used for measurements in the SFA.

In this work, normal (adhesive) interactions between well characterized, highly stretched molten brush layers created by Langmuir–Blodgett (LB) technique are studied. The distinguishing features of these brush layers are high monodispersity, high grafting density and relatively high molecular weight of the chains, all resulting in high stretching of the molecules. They also have an advantage of a well-characterized structure regarding the interanchoring spacing and brush height, which can be deduced straightforwardly from the deposition procedure.

2. EXPERIMENTAL

2.1. Polymer

Linear polyisoprene (PI) end-terminated by the zwitterionic group $-(CH_3)_2N^+(CH_2)_3SO_3^-$ (–X) is used to obtain stretched brush monolayers (its structure is in the inset to Fig. 4a). It was synthesized via anionic polymerization. The details on synthesis and characterization of the polymer are given elsewhere [15]. The molecular characteristics of the end-functionalized PI are: M_n = 28 300 (membrane osmometry); M_w = 29 900 (small-angle laser light scattering), M_w/M_n = 1.06 (size exclusion chromatography), indicating high monodispersity of the macromolecules.

The polymer is amorphous, of honey-like viscosity at room temperature, T_g= –66°C [16], the unperturbed radius of gyration $R_g = (0.8M_w^{1/2}) = 137$ Å [17], viscosity $\eta_0 = 9.38 \times 10^{-14} M_w^{3.66}$ = 230 Pa s at the temperature of our experiments (25°C), surface tension of pure polyisoprene is reported as 31 mN/m, and the density of the polymer ρ = 0.913 g/cm^3 [18].

2.2. Apparatus and Experimental Procedure

2.2.1. Langmuir–Blodgett (LB) technique. The monolayers of PI–X for SFA studies were prepared using a 36 × 15 cm rectangular Langmuir–Blodgett minitrough made of polytetrafluoroethylene and equipped with two compression hydrophilic barriers and Wilhelmy Pt plate for the detection of surface pressure π. It is also supplied with dipper device (KSV, Finland, Fig. 2). The water used (resistivity 18.2 × 10^6 Ω/cm, total dissolved organic carbon <4 ppm) was purified by a Millipore system.

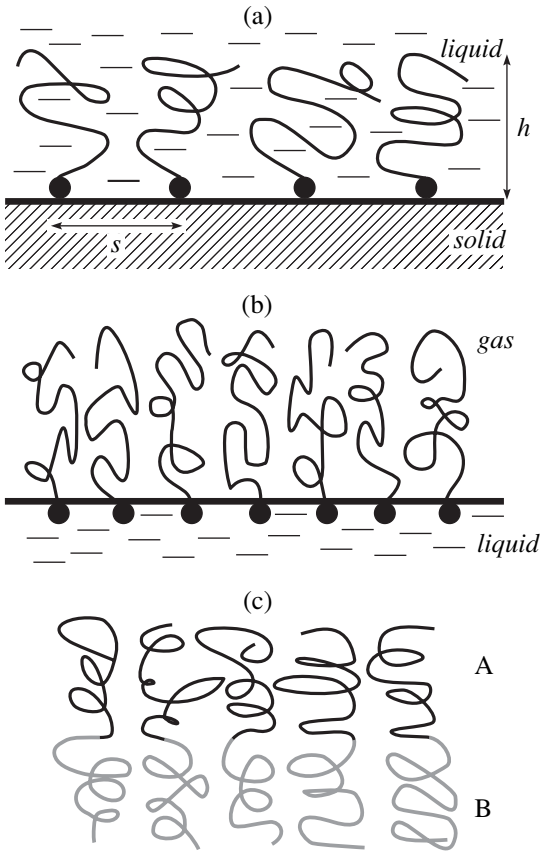

Fig. 1. Schematic comparison of (a) monolyers of tethered polymers (polymer brushes) swollen with solvent, where *h* is the brush height and *s* is the lateral spacing between the grafted chain ends; (b) monolayers of tethered polymers that are free of solvent (polymer brush melts), (c) one lamella of a phase-separated A–B block-copolymer.

Polymer was spread over the surface of pure water from 0.01 wt % solutions in hexane (Merck, spectroscopic grade). After the evaporation of the solvent, the layer was compressed to a predetermined pressure. Prior to deposition, the stability of the layer was checked over a 10–15 min period. All depositions were carried out by withdrawing the substrates from the water subphase at constant pressure 15 mN/m and 2 mm/min withdrawal speed. Freshly cleaved mica sheets (Ruby Clear Muscovite mica, Grade 1, S & J Trading Inc., N.Y.) glued to glass lens (EPON 1004 epoxy glue) were used throughout as substrates. Deposition on both lenses was carried out simultaneously. The transfer ratio, determined in separate experiments with rectangular mica sheets, was close to unity. We note that, upon withdrawing the lenses from the water surface, a residual interfacial layer of water may remain on mica,

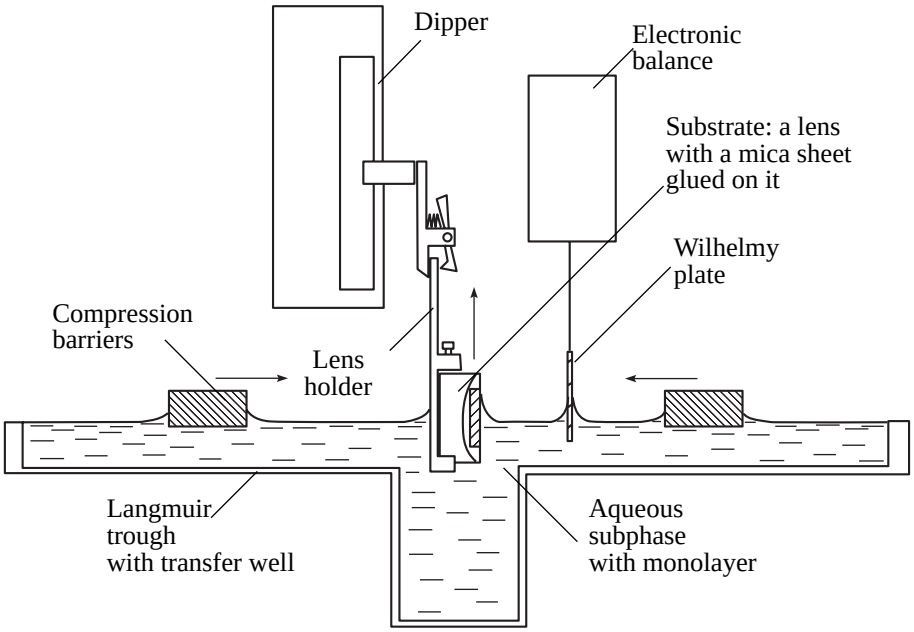

Fig. 2. Schematic of the Langmuir–Blodgett trough with illustration of the monolayer deposition onto mica sheets glued to quartz lenses.

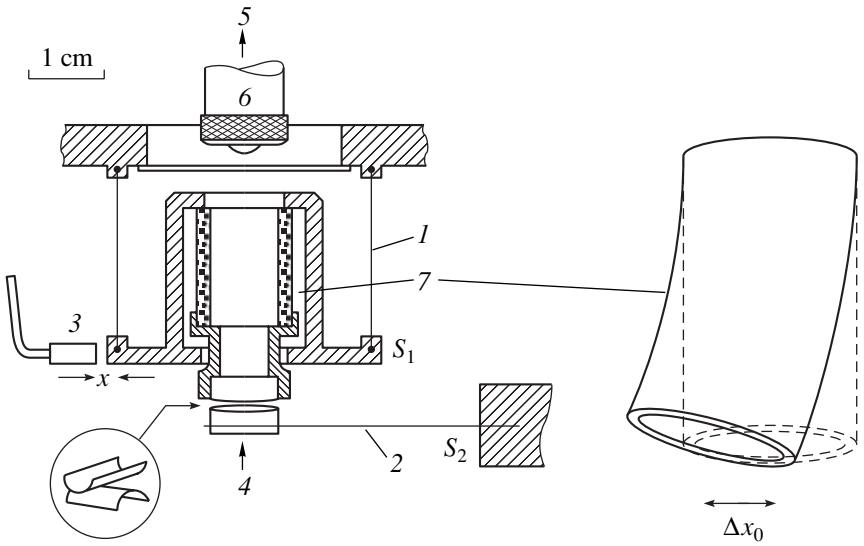

Fig. 3. Schematic of the surface force apparatus used in the present experiments. The two mica sheets are mounted on cylindrical quartz lenses in a cross-cylinder configuration (inset). Heat filtered white light (*4*), passing through the SFA, interferes in the contact area, and then it is transmitted to spectroscope (*5*) through the microscope tube (*6*). The top lens is mounted on a sectored piezoelectric tube (*7*). Normal forces are measured via the bending of the horizontal stainless still leaf spring S_2 (*2*). Bending of the shear-force spring S_1 (*1*) is monitored by an air-gap changes in the capacitor probe (*3*).

protected by the thick polymer film from drying using conventional procedures (e.g., P_2O_5).

2.2.2. Surface forces measurements. The surface force apparatus used in this study has recently been described in detail [19]. This version of SFA has particularly high sensitivity and resolution in measuring lateral displacements and shear forces. Figure 3 shows the SFA schematically.

SFA measures normal forces $F(D)$ and lateral (shear) forces $F_s(D)$ between two curved mica sheets positioned in a cross-cylindrical configuration a closest distance D apart. The gap between mica sheets is determined using a multiple beam interferometry with an accuracy of about ±3 Å [20]. This is done by monitoring the change in the wavelength of fringes of equal chromatic order (FECO) in response to applied motion

in the direction normal to the surfaces. The gap between mica sheets can be filled with air, solvent or solution. The surfaces may be covered with adsorbed layers or deposited films like in our case. Distance D between mica surfaces is then calculated via interferometric equations using the refractive index of certain media between the mica sheets.

The forces are measured by monitoring the bending of two orthogonal sets of leaf springs: vertical spring S_1 (spring constant K_1 = 300 N/m), and horizontal spring S_2 (spring constant K_2 = 150 N/m). The bending of S_2 (on which the lower lens is mounted) is determined with the multiple beam interferometry. Relative normal motion of the surfaces was affected via a three-stage mechanism, with the most delicate stage utilizing a sectored piezoelectric tube (PZT) which could ensure both normal and lateral motions. The area of flattened contact was measured to characterize the geometry of the interacting areas. In a number of cases, the images of fringes were taken using a video camera to illustrate the topography of the contact.

2.2.3. Adhesion and interfacial energy measurements. Since the lower lens is suspended at the end of a cantilever spring, regions where the gradient of the force $dF(D)/dD$ is larger than the spring constant K_2 are inaccessible. At the distance where such intrinsic instabilities occur, the surfaces will jump to contact driven by the attractive dispersion forces or jump out when pulled apart. The value of the pull-off force, F_p, needed to separate the two contacting surfaces, can be determined by multiplying the jump-out distance by the spring constant K_2.

The polyisoprene/air surface energy γ_p may be determined according to the Johnson, Kendall and Roberts (JKR) equation [21]:

$$\gamma_p = -F_p/3\pi R \quad (1)$$

where R is the radius of the curvature (≈1 cm) of the surfaces prior to contact.

The radius of the flat contact area a_{exp} is measured directly from the fringe shape. It was generally in the 15–25 μm range.

2.2.4. The experimental procedure. In each experiment, the mica sheets were glued onto the cylindrical lenses and mounted into the SFA. Then the FECO wavelengths for air contact between the bare mica surfaces were calibrated. Following this, the apparatus was opened in a dust-free laminar flow hood, the lenses dismounted and fixed in the lens holders of the LB device (Fig. 2), and the deposition of the PI–X monolayer was carried out. The lenses were then mounted back in the apparatus as close as possible to their original position. Prior to force measurements, the polymer layers were dried inside the box under the flow of dry nitrogen for several hours and experiments were carried out under a dry nitrogen atmosphere. During the approach, the surfaces were moved slowly toward each other using the PZT until they jumped into contact from a position roughly 50–100 Å from the polymer-polymer contact. No external compression load was applied following this jump into the adhesive contact.

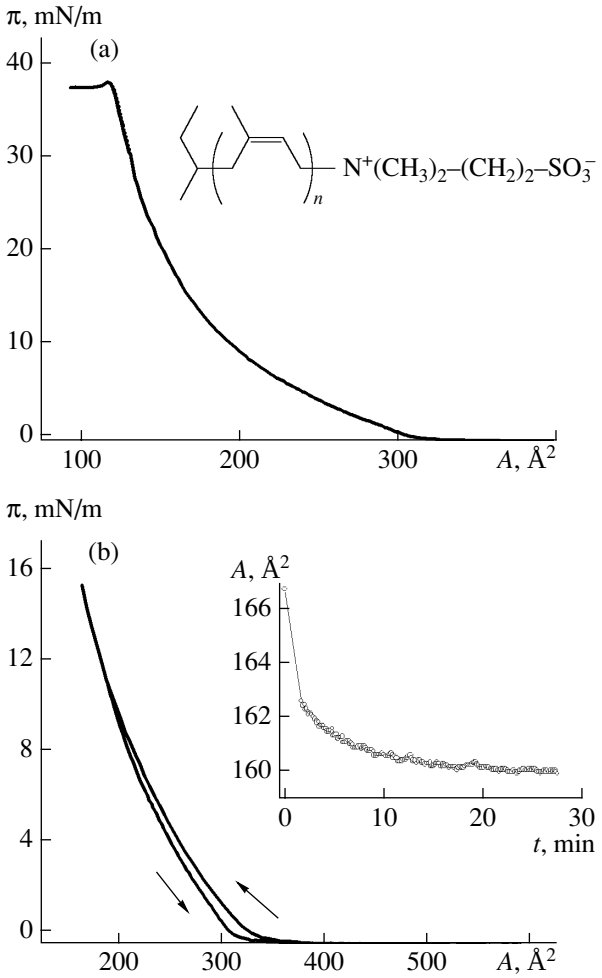

Fig. 4. (a) The typical π–*A* isotherm of PI–X on the water subphase. Inset: polyisoprene end-terminated by the zwitterionic sulfo-amino group. (b) The compression and expansion isotherms of the PI–X monolayer showing insignificant histeresis. Inset: Kinetics of a PI–X monolayer stability showing the area per molecule versus time at constant surface pressure 15 mN/m.

Results shown are from several different experiments, with data taken from a number of different contact positions in each experiment.

3. RESULTS AND DISCUSSION

3.1. PI–X Monolayers at the Water/Air Interface

Monolayers from end-functionilised polymers can be regarded as a continuous film of uniform thickness that is free of solvent and that has one interface with the aqueous phase and another, with the air (Fig. 1b). All polymer chains are bound to the aqueous phase by one end (the functional group). The system is characterized by the area S of this interface, the temperature T, the

number of polymer chains in the system n, and the properties of polymer chains. The measured film pressure is given by the difference between the derivatives of the free energy with respect to the area of the pure water surface and the adsorbed polymer film:

$$\pi = -(\partial F/\partial S)_{T,\, n(\text{polymer film})} + (\partial F/\partial S)_{T(\text{water/air interface})}. \quad (2)$$

The second term in Eq. (2) is just the surface tension of pure water γ_w. The first term in Eq. (2) can be represented by the sum of the following three contributions: (1) the interfacial tension at the polymer/air interface, (2) the interfacial tension at the polymer/water interface, and (3) a contribution to the surface pressure due to an elastic stretching of the polymer chains, $(\partial F/\partial S)_{\text{elastic}}$. Under the assumption that the free ends of the chains are similar to the other segments and do not influence the surface tension of the interfaces, the first contribution is independent of the area per molecule and is just a polymer surface tension γ_p that is a constant.

The head groups of the polymer chains, however, are chemically different from the polymer chain, and the surface concentration of these groups does influence the interfacial tension of polymer/water interface γ_{pw}^0. In principle, the addition of the zwitter-ionic groups tends to lower γ_{pw}^0:

$$(\partial F/\partial S)_{\text{water/polymer}} = \gamma_{pw}^0 - f(S/n). \quad (3)$$

Summarizing all the above considerations, one can obtain the following expression:

$$\pi = \gamma_w - (\gamma_p + \gamma_{pw}^0) + f(S/n) - (\partial F/\partial S)_{\text{elastic}}. \quad (4)$$

The elastic component of the surface pressure was first developed theoretically by Heger and Goedel [13]. They also confirmed experimentally that there is a regime of stable polymer brush melts on water surface when the polymer chain statistics dominate the properties of the film. This conclusion means that the polymer monolayers retain the intrinsic polymer properties and could be considered as a model of polymer brush melts.

A typical isotherm of PI–X monolayer, shown in Fig. 4a, can be characterized as an isotherm of an expanded type, with collapse pressure above 37 mN/m. To obtain complete spreading, it is necessary to use highly dilute (no less than 0.01 wt %) solutions of end-functionalized polymers. This condition is dictated by the "critical association concentration" (10^{-6}–10^{-7} molar concentration of zwitterions), which was determined by dynamic light scattering measurements of PI-X dilute solutions in aliphatic solvents [1]. The reasons for the poor spreading of PI-X from more concentrated solutions have been discussed in [13]. The authors suggested that, in the bulk of the polymer phase, polar end groups form clusters, which do not totally dissociate when dissolved in a nonpolar solvent. Thus, polar groups are sterically hindered from accessing the water surface. In this case, the isotherm shifts to lower areas per head group. If dilute solution is used, the monolayer is laterally homogeneous and the isotherms are independent of spreading conditions, compression speed and are nearly free of hysteresis (Fig. 4b). Measurements of the kinetic stability of the PI-X monolayers at the deposition pressure (inset to Fig. 4b) confirmed that such layers are stable enough to be transferred onto solid substrates, resulting in a reproducible well defined brush melt monolayer. The monolayer was stable during almost 30 min of measurements at a constant surface pressure of 15 mN/m, when the value of the area per molecule decreased only by 4%.

Since the transfer ratio while depositing onto the solid substrate was close to unity, we may assume that the surface density of the monolayer is preserved, and we obtain on a freshly cleaved mica surface a well defined highly stretched brush melt composed of near monodisperse polymer chains with $N_w \approx 427$ monomers. The amount of polymer per unit area and the layer thickness are determined from the parameters of compression isotherm during deposition. That is, at a surface pressure of 15 mN/m, the area per molecule A was 170 ± 6 Å^2. The thickness h of each monolayer is obtained directly from the incompressibility condition:

$$h = (M_n/N_A)/\rho A, \quad (5)$$

where M_n and ρ are the molecular weight and density of the polymer, and N_A is Avogadro's number. At M_n = 28 300 and $\rho = 0.913$ kg/m^3, $h = 302 \pm 10$ Å. The contact separation following the jump-in of the two mica surfaces each covered with PI-X monolayer, averaged from several experiments is 560 ± 20 Å. If we assume that this value represents twice the thickness of an incompressible monolayer, this would correspond to each monolayer being on average 280 ± 10 Å. The two values of the monolayer thickness obtained by completely different absolute approaches, are close to agreeing within their scatter.

Other relevant parameters of the PI-X brush melt are the polymer adsorption $\Gamma = 30$ mg/m^2, the surface number density of end groups (number of molecules per unit area) $\approx 0.59 \times 10^{18}$ m^{-2}, and the mean distance between grafting ends, $s = \sqrt{A} \approx 13$ Å (compared to the unperturbed end-to-end dimension of the chain, $R_0 = 137$ Å). The ratio of the brush extension (280 Å in the film) to the interanchor spacing turned to be very appreciably higher than in most studies of solvated brushes.

When transferred via the LB technique onto mica substrate, the PI-X monolayers expose an outer brush layer of chain ends to the air, the polar zwitterionic head groups being attached to the solid surface. From earlier studies, we know that the interaction energy $\varepsilon_{\text{zwitterion/mica}}$ of the zwitterions with mica in a toluene medium is ca. 7–8 k_BT [22]. We may assume that this value remains similar in a melt. The total energy asso-

ciated with the PI chains in the brush stretched to an extent h is to a good approximation given by their stretching energy $E_{stretch}$, as there is no osmotic contribution in the melt. This is given by $E_{stretch} = (3h^2/2R_0^2)k_BT \approx 6k_BT$, comparable to or slightly lower than the zwitterion–mica sticking energy. Moreover, the tension within each chain is of order $(\partial E_{stretch}/\partial h) \approx 0.05(k_BT/\text{Å})$ [2]. This compares with the much larger tension of order $(\varepsilon_{zwitterion/mica}/2\ \text{Å}) \approx 4(k_BT/\text{Å})$ required to detach a zwitterion end-group from the substrate, since pulling it away by say 2 Å from the mica surface presumably overcomes most of the sticking energy and so suffices to detach it.

Thus, we would not expect the anchoring zwitterion ends to be readily removed from the mica surface due to the relaxation of the stretched conformation of the chains. Moreover, the destabilization of the brush monolayer due to the desorption of chain ends is kinetically inhibited by the high viscosity of the PI-X melt. This is indeed consistent with our observation that, over the time scale of our experiments, the initial film thickness and interactions, both normal and shear, remained generally the same.

3.2. Opposing Brushes between Mica Surfaces

3.2.1. Kinetics of film thinning. On approaching the surfaces covered with PI-X monolayers spontaneously jump-in to a well-defined flattened contact with the averaged radii of about 15–25 μm. The effective attraction observed for the brush covered surfaces can be explained by the gain in the free energy, when two brush/air interfaces are replaced by a sole brush/brush interface with a lower surface energy. Already during the first minutes after the contact was formed, the polymer film starts to thin spontaneously. The gradual change with time in the position of a given fringe for a bilayer in contact is shown in Fig. 5. Even fringes, which are more sensitive to the differences in the refractive indices of the medium and the polymer film at the surface separations of our experiments, exhibit a characteristic "neck" which thickens with time, as shown in Fig. 5c. The right of Fig. 5 shows a cartoon corresponding to the geometry of the melt brushes in contact.

The size and the shape of the flat contact zone immediately after the jump-in are in a reasonable agreement with the JKR theory (Fig. 5b), which in the absence of an applied normal load relates the radius a of the contact zone to the underformed radius of curvature ($R \approx 1$ cm) of the mica surfaces as

$$a^3 = 12\pi\gamma_p R^2/K, \qquad (6)$$

where K is the effective bulk modulus of the PI-X-monolayer/mica/glue/glass system and has a value in the range $K \approx (1–5) \times 10^9$ N/m^2 [19], while γ_p is the surface energy of the PI monolayer. Putting $\gamma_p = 31$ mJ/m^2 gives $a \approx 30–50$ μm, which is comparable with our observations ($a_{exp} = 15–25$ μm). The two-fold variance in the measured diameter of the flat contact zone may be due to the differences in the local thickness of the glue layer used to mount the mica sheet to the cylindrical glass lens or to local variations in the effective radius of curvature R.

Figure 6a shows the thinning of the polymer bilayer as a function of time following spontaneous monolayer jump into contact. Kinetic curves of the film thinning are quite reproducible for different contact positions and experiments (Fig. 6b), and can be well fitted by the exponential second order decay (solid line in Fig. 6a) for the initial and following thinning regimes. From Fig. 6a, it can be seen that, during the first minute after the jump-in, film thickness decreases by 25 ± 5 Å. During the next 10–20 min, the brush bilayer loses about 20% of its initial thickness. After 10–20 min, the flow of the brush melt out of the gap becomes more sluggish with thinning velocity about 1 Å/min. In 2–3 h, the film thickness decreases to about 300 Å. The residual film thickness corresponds to the asymptotic value D' in the fitting equation

$$D = D' + A_1\exp(-t/t_1) + A_2\exp(-t/t_2), \qquad (7)$$

and it is about 290 ± 35 Å. This possibly means that, at longer periods, polymer chains are not squeezed out totally from the gap. Rather the brushes finally assume the conformation dictated by the minimum of the free energy.

We emphasize that, throughout the experiments, external load was never applied to the surfaces following their jump into contact. However even in the absence of such a load, the JKR theory tells us that, under adhesive forces, two contacting bodies experience a "contact-induced" normal stress, with a compressive maximum in the center of the contact zone decreasing to negative (tensile) values toward the edges. We note here that the compressive pressure at the center of the contact zone estimated from the JKR theory for our system is of order 10 MPa (100 atmospheres) [23].

We attribute the thinning of the brush melt to the lateral pressure gradient arising from the normal stress, which must cause the zwitterion groups anchoring the chains to the mica to migrate laterally away from the contact-zone midpoint (where the pressure is the highest, Fig. 7). As a result of such migration, the surface coverage decreases. Similar effect of the monolayer fluidity and ambient conditions on the enhanced lateral diffusion and adhesion of the end-adsorbed short-chain surfactants was studied by Chen and Israelachvili [23]. However in their experiments, the absolute changes in the monolayer thickness have been too small to make any systematic kinetic measurements. As it was already mentioned earlier, in our system a residual interfacial layer of water may remain on mica surface after the deposition procedure, which could facilitate the lateral sliding of the chain ends.

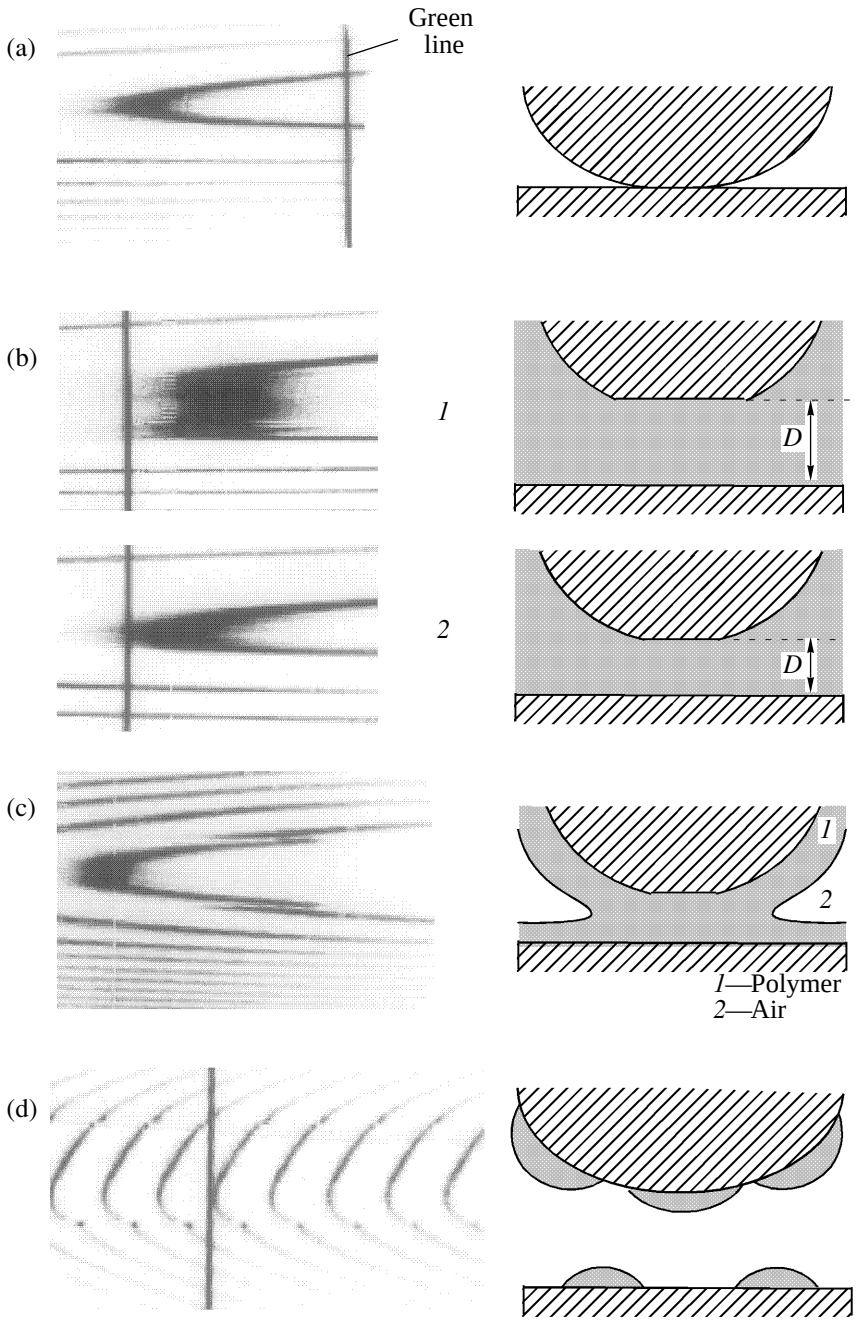

Fig. 5. Images of the ECO fringes, taken with a video camera and corresponding sketches of the contact. (a) Direct contact between mica sheets in the air taken as a calibration of the zero separation between the surfaces ($D = 0$). The vertical line is a reference green line (Hg). (b) Images of a certain even fringe, taken at time t: (*1*) 7 and (*2*) 30 min and corresponding to the polymer film thickness *D*: (*1*) 532 and (*2*) 427 Å. (c) Image of an odd fringe showing characteristic "neck." (d) Image of the fringes after the jump out of the adhesive contact.

3.2.2. Adhesion measurements. The use of the JKR expression (Eq. (1)) to evaluate surface energies is complicated when the surfaces are viscoelastic (which is the case for polymer monolayers above the T_g of polyisoprene, as in this study) due to pull-off-rate dependence of the force F_p needed to separate the surfaces from the contact. Recent SFA studies on the rate-dependent pull-off forces in thin layers of block-copolymers, one block of which is represented by polyisoprene [12, 24], have been carried out to probe the viscoelastic adhesion mechanism in these polymer melt films. We observed some similarities to this in the behavior of the PI-X brush melt on separation from adhesive contact, as well as some different features.

On separation from the flattened contact between PI-X brush monolayers, the contact area gradually

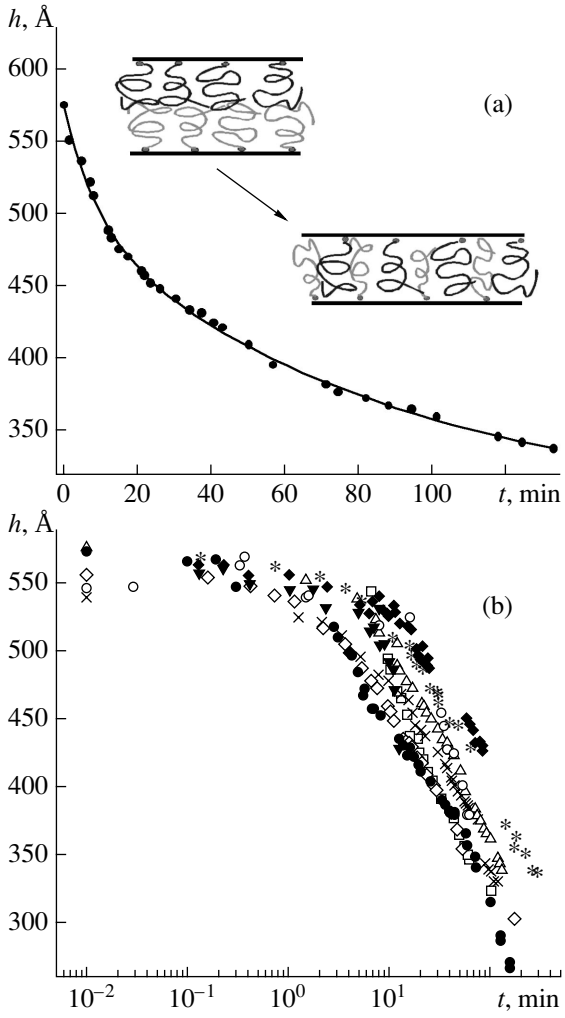

Fig. 6. (a) Kinetics of the two opposing brush melts thinning following the jump-in to adhesive contact. The solid line corresponds to the function (Eq. (7)) $D = (285 \pm 65) + (75 \pm 30)\exp(-t/(8 \pm 4)) + (197 \pm 60)\exp(-t/(116 \pm 78))$ (t in min, D in Å). Inset: Possible molecular structures of the brush bilayer following the jump-in and at the end of kinetic measurements. (b) Kinetics of the film thinning for different contact positions and experiments plotted in logarithmic scale.

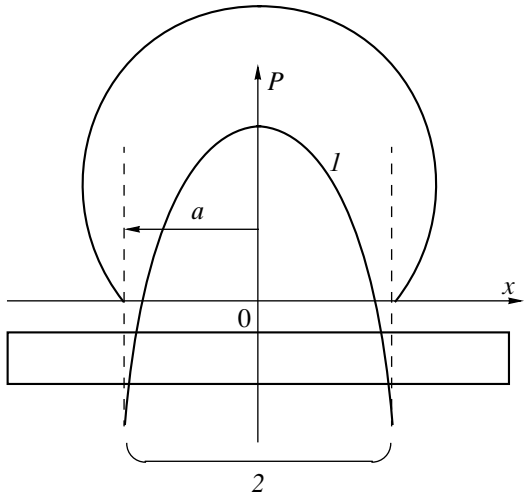

Fig. 7. Schematic of the stress distribution P (*1*) in an adhesive flattened contact (*2*) of area a under a compressive load F according to the JKR theory.

decreases. Finally it appears as a point just before the jump out occurs. This point deformation is very pronounced, and is accompanied by the slow expansion of the film by up to 50–70 Å in a manner suggesting the formation of a thin neck. The formation of such a point deformation on receding may be due to the nonuniform stress distribution within the contact zone (Fig. 7), which leads to a higher degree of interdiffusion and entanglements, and, hence, of adhesive energy towards the center of the contact zone.

In contrast to previous studies [12, 24] which have shown an increase of over 50% in the surface energies determined from the pull-off values compared with their thermodynamic values, we did not measure a similar enhancement in our investigation. The origin of the anomalously higher values in these earlier studies is believed to be an effectively-enhanced adhesion resulting from viscoelastic effects at the finite pull-off rates between the mutually-interpenetrated polymer-melt layers on the opposing surfaces. In our experiments, the surface energy of each brush layer determined from the pull-off force via Eq. (1), was about 33 ± 5 mN/m, similar to the literature value of surface tension for bulk polyisoprene (γ_p = 31 mN/m) [18]. The apparent absence of any enhancement of the pull-off force due to energy dissipation while viscous friction of the chain ends in the contact zone can be understood by the damage of the brush structure while applying of the decompression load or by the high enough separation of the monolayers from the contact.

We observed that each time, following the jump out, the ECO fringes, which map the relative contact geometry, appeared to show discontinuities (Fig. 5d). This indicates that the layers are no more uniform (as otherwise the fringes would be smooth and continuous) due to probably partial detaching of the end-groups from the mica surface or due to partial dewetting of the film, as shown schematically in Fig. 5d. As it was shown earlier, the weakest place of the grafted chains structure is the polymer/solid interface [25]. Probably, the "crack" line avoids the regions of highly interpenetrated and entangled chains from the opposing layers, resulting in a partially peeled film. Thus, it is not strictly correct to use Eq. (1) for the calculation of adhesion between PI-X monolayers, and the fact that our measured value is actually close to the thermodynamic value for γ_p is rather fortuitous.

3.3. Single PI-X *Brush Trapped between Mica Surfaces*

In order to get closer understanding of the mechanism of the spontaneous film thinning, the experiments

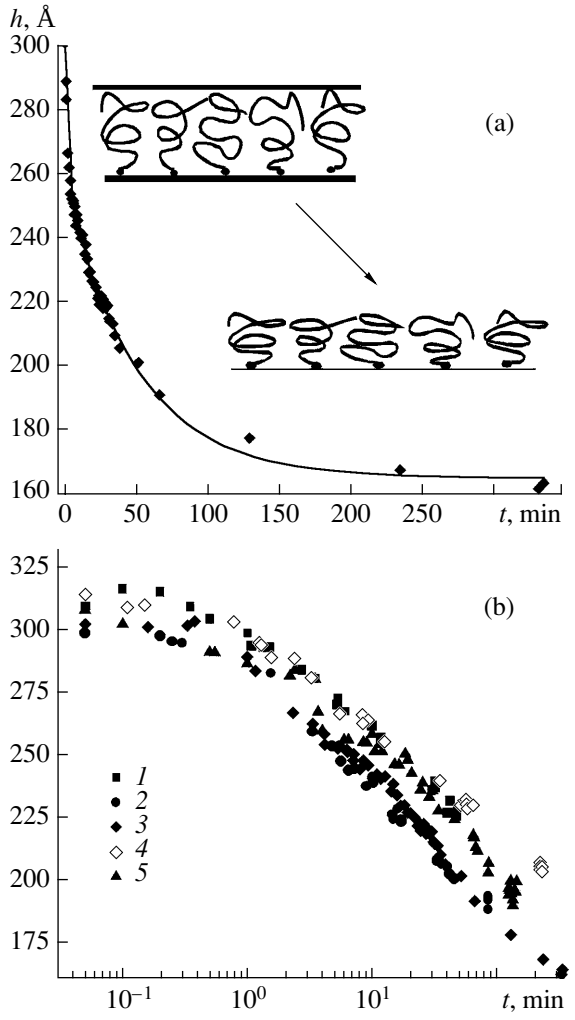

Fig. 8. (a) Kinetics of the PI-X brush monolayer thinning following the jump-in to adhesive contact. The solid line corresponds to the function (Eq. (7)): $D = (180 \pm 22) + (47 \pm 16)\exp(-t/(3.4 \pm 3)) + (71 \pm 18)\exp(-t/(65 \pm 34))$ (t in min, D in Å). Possible molecular structures of the brush monolayer following the jump-in and at the end of kinetic measurements are shown as insets. (b) Kinetics of the brush monolayer thinning measured after the aging of the film for (*1*) 25, (*2*) 9, (*3*) 5, (*4*) 2 and (*5*) 1 days after deposition.

have been done in which brush layer was deposited only on one mica surface. In this case, we also observed a jump-in, flattening of the contact, and spontaneous thinning of the brush monolayer. The surface separation following the jump-in was 305 ± 6 Å, close to the calculated brush thickness $h = 302 \pm 10$ Å. The thinning behavior $D(t)$ with time shown in Fig. 8 resembled that of the brush bilayer, suggesting the similarity of the thinning mechanism. The fitting parameters of the exponential decay (solid line in Fig. 8a) are approximately twice smaller than for the two opposing brushes. The radius of the flattened contact area for the monolayer just after the jump-in was generally smaller than for the bilayer case (a_{exp} = 10–15 μm). However, it should be noted that the shear behavior of the monolayer was found to be principally different from that of the bilayer film [26].

An important observation, which we deduced from the kinetic measurements, is the stability of the polyisoprene monolayer toward cross-linking and dewetting from the mica surface. Usually measurements were completed within a couple of days to avoid dramatic changes to the specific brush architecture in the monolayer. Measurements on one sample have lasted for 25 days, when the box was kept in clean nitrogen environment and shortly exposed to white light for measurements. As seen from Fig. 8b, the initial thickness of the film, as well as the kinetic curves of the monolayer thinning are within the scatter we normally had for different contact positions. Moreover, the homogenous shape of the fringes on approach and in contact also confirmed the stability of the monolayer.

Another argument in favor of the high physical stability of the LB monolayers from PI-X was obtained by the AFM measurements of the monolayer, which showed homogeneous surface with the mean roughness of about 5 Å (Fig. 9). This investigation did not reveal any signs of dewetting or inhomogeneous domains even after 6 months of aging in a clean dry atmosphere.

3.4. Mechanism of Contact Thinning

Earlier we presented a simplified treatment based on the JKR model to evaluate the total compressive force F_0 acting on the molten brush monolayers in adhesive contact [27]. Here, we make use of the result of this treatment to consider further the process leading to the thinning of the brush layers when in adhesive contact.

We now assume that we may apply the hydrodynamic Reynolds's equation [28] relating the approach rate (dD/dt) of a disk of radius r_0 parallel to a flat surface a distance D away ($D \ll r_0$), when compressed at pressure P across a liquid of viscosity η (Fig. 10):

$$dD/dt = -2D^3P/(3\eta r_0^2). \quad (8)$$

In order for this to be valid for the compression of the melt brushes in a thin gap between two disks of radius r_0, we have to assume, first, that the contact pressure is uniformly distributed within the contact area when the contact is formed, and, second, that the pressure distribution holds the hydrodynamic conditions of the extrusion of a liquid film from a gap described by the geometry of a disk and a flat surface, as in Fig. 10. Then we can substitute in Eq. (8) for the pressure, calculated from the total compressive force F_0 acting on the molten brush monolayers in adhesive contact:

$$P = F_0/(\pi r_0^2). \quad (9)$$

This is a simplification in view of the strong pressure maximum in the center of the contact disk. Nevertheless, if we substitute in (8) for (9) we obtain

$$dD/dt = -2D^3F_0/(3\eta\pi r_0^4). \quad (10)$$

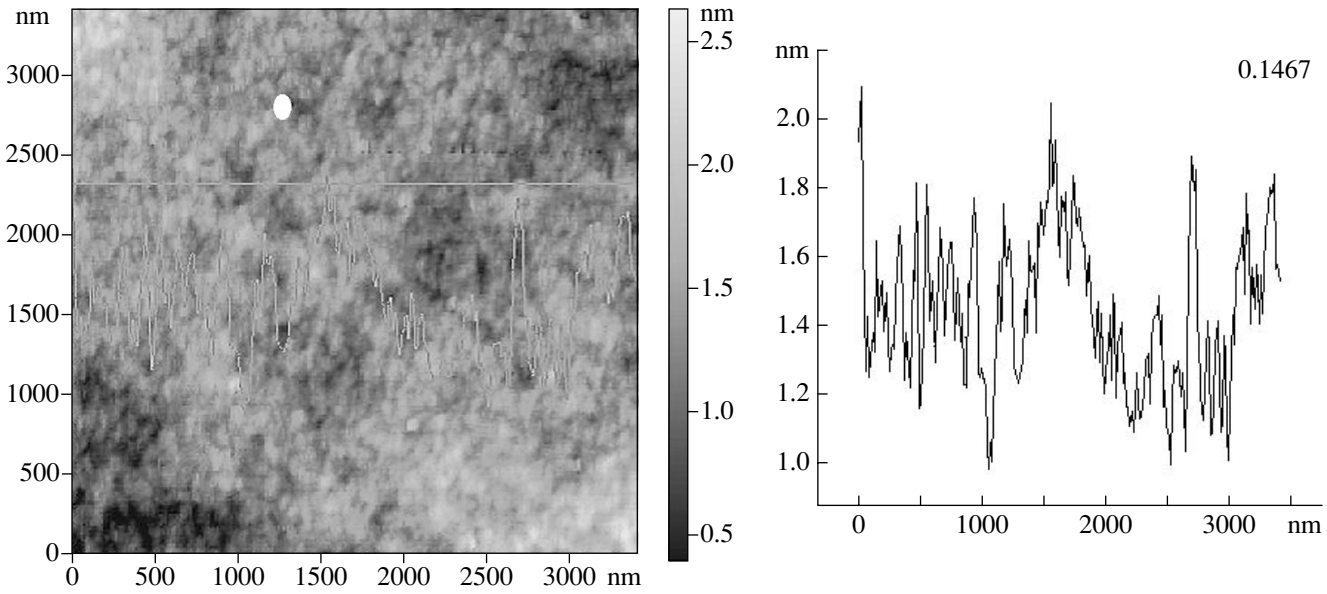

Fig. 9. AFM image of the PI-X brush melt aged during 6 months.

For more convenient analysis of the experimental data, we integrate Eq. (10) using boundary conditions $D_{t=0} = D_0$ and $D(t) = D_t$:

$$(3\pi r_0^4/4)[1/D_t^2 - 1/D_0^2] = (F_0/\eta)t. \qquad (11)$$

This method is frequently used to measure molecular forces and disjoining pressure in foams or surfactant thin films, and even to calculate the Hamaker constant [29]. For relatively thick films, which are our case, P is determined mainly by the changes in the Laplace pressure. In this case, function $(1/D_t^2 - 1/D_0^2) = f(t)$ should be a straight line going through zero. Any deviations from the linear dependence can provide information on the thinning mechanism, in particular on the relaxation of the elastic compressive stress in PI-X brush monolayers. Figure 11 shows the linearized dependence (using Eq. (11)) of film thickness D versus the duration of the contact for PI-X brush melt bilayer and monolayer. In this case, the slope of the curve represents the relation between the compressive force and effective viscosity of the polymer film [Eq. (11)].

It was shown earlier [26] that the kinetics of extrusion of the polymer film in the first seconds following the jump-in can be adequately described by the suggested model putting in Eq. (10) the bulk viscosity of polyisoprene. Here we present a more detailed analysis,

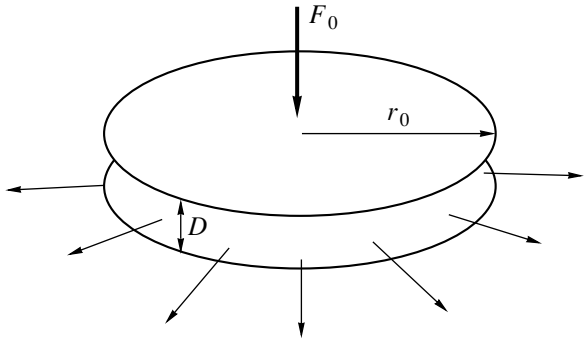

Fig. 10. Schematic of the extrusion of a liquid film out of the thin gap D between two flat disks of radius r_0 under the normal load F_0 and the geometry of the contact relevant to Eqs. (9)–(11).

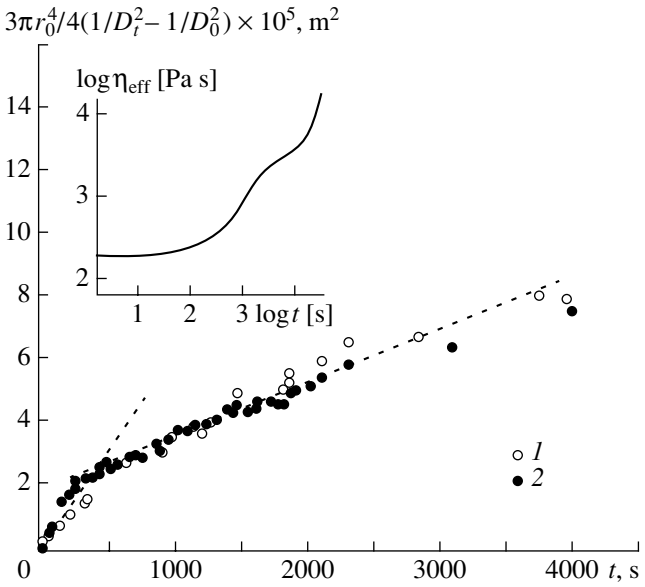

Fig. 11. Kinetics of the polymer film thinning, linearized using Eq. (11) for (*1*) the PI-X brush melt bilayer and (*2*) monolayer. Inset: schematic of the displaced bilayer viscosity versus time.

which shows that the effective viscosity of the film in the gap grows fast from its initial value to much higher value (inset to Fig. 11). We may, at this level of approximation, estimate the compressive force according to the relation $F_0 = C\gamma_p R$ with $C \approx 4.6$, $\gamma_p = 31$ mJ/m^2 and $R = 1$ cm [27]. Putting these values in Eq. (11), we obtain the value of the effective viscosity of the PI-X films (about ten minutes after the jump-in) of order of 10^3 Pa s, which is an order of magnitude higher than the viscosity of bulk polyisoprene of the same molecular weight (230 Pa s). This result is very much in line with earlier observations on increased viscosity in thin films in a gap compared to the bulk values of the same material [19, 30–32].

Interestingly, the linearized kinetic curves for the monolayer and bilayer of brush melts are very close to each other in the initial and intermediate period of the contact. On molecular level, it means that the differences in the polymer film architecture do not enter the thinning mechanism following the jump-in.

4. CONCLUSIONS

Dense PI-X melt brush layers (an order of magnitude denser than in previous melt brush studies) were created on mica via the LB deposition. Their integrity, thickness and behavior on confinement once they had come into adhesive contact were determined using an SFA both for bilayers (a brush on each interacting mica surface) and for a monolayer (a single brush layer facing a bare mica surface). Once the layers had jumped into adhesive contact, the progressive thinning of the confined melt brushes occurred, slowing down from an initially rapid rate. The residual film thickness after a few hours of extrusion of the polymer brushes from a gap is (0.5–0.7) of their initial thickness. The presented model for the polymer film extrusion from the small gap is based on the idea that compressive contact pressure in the adhesive contact provokes the chains to move laterally via the sliding of the zwitterionic anchoring groups on the surfaces. The kinetics of thinning of the layers can be quantitatively described using a simplified treatment based on the JKR model together with a Reynolds equation describing the extrusion of a liquid from a flat gap.

ACKNOWLEDGMENTS

P. Protsenko thanks the Karyn Kupcinet International Science School (WIS) for financial support.

REFERENCES

1. Davidson, N.S., Fetters, L.J., Funk, W.G., *et al.*, *Macromolecules*, 1988, vol. 21, p. 112.
2. Milner, S.T., *Science* (Washington, DC), 1991, vol. 251, p. 905.
3. Milner, S.T., Witten, T.A., and Cates, M.E., *Macromolecules*, 1988, vol. 21, p. 2610.
4. Halperin, A., Tirrel, M., and Lodge, T.P., *Adv. Polym. Sci.*, 1992, vol. 100, p. 31.
5. Napper, H.D., *Steric Stabilization of Colloidal Dispersions*, London: Academic, 1983.
6. Fleer, G.J., Cohen-Stuart, M.A., Scheutjens, J.M.H.M., *et al.*, *Polymers at Interfaces*, London: Chapman and Hall, 1993.
7. Yerushalami-Rosen, R., Klein, J., and Fetters, L.J., *Science* (Washington, DC), 1994, vol. 263, p. 793.
8. Klein, J., Kumacheva, E., Mahalu, D., *et al.*, *Nature* (London), 1994, vol. 370, p. 634.
9. Klein, J., *Annu. Rev. Mater. Sci.*, 1996, vol. 26, p. 581.
10. Karim, A., Satija, S.K., Douglas, J.F., *et al.*, *Phys. Rev. Lett.*, 1994, vol. 73, p. 3407.
11. Ruths, M., Johannsmann, D., Ruhe, J., and Knoll, W., *Macromolecules*, 2000, vol. 33, p. 3860.
12. Watanabe, H. and Tirrell, M., *Macromolecules*, 1993, vol. 26, p. 6455.
13. Heger, R. and Goedel, W.A., *Macromolecules*, 1996, vol. 29, p. 8912.
14. Baltes, H., Schwendler, M., Helm, C.A., *et al.*, *Macromolecules*, 1997, vol. 30, p. 6633.
15. Pispas, S., Pitsikalis, M., Hadjichristidis, N., *et al.*, *Polymer*, 1995, vol. 36, p. 3005.
16. Widmaier, J.M. and Meyer, G.C., *Macromolecules*, 1981, vol. 14, p. 450.
17. Hadjichristidis, N., Zhongde, X., and Fetters, L.J., *J. Polym. Sci., Part B: Polym. Phys.*, 1982, vol. 20, p. 743.
18. *Polymer Handbook*, Brandrup, J., Immergut, E.H., and Grulke, E.A., Eds., New York: Wiley, 1999.
19. Klein, J. and Kumacheva, E., *J. Chem. Phys.*, 1998, vol. 108, p. 6996.
20. Israelachvili, J.N., *J. Colloid Interface Sci.*, 1973, vol. 44, p. 259.
21. Johnson, K.L., Kendall, K., and Roberts, A.D., *Proc. R. Soc. London, A*, 1971, vol. 324, p. 301.
22. Taunton, H.J., Toprakcioglu, C., Fetters, L.J., and Klein, J., *Macromolecules*, 1990, vol. 23, p. 571.
23. Chen, Y.L. and Israelachvili, J.N., *J. Phys. Chem.*, 1992, vol. 96, p. 7752.
24. Ruths, M. and Granick, S., *Langmuir*, 1998, vol. 14, p. 1804.
25. Klein, J., Kumacheva, E., Perahia, D., and Fetters, L.J., *Acta Polym.*, 1998, vol. 49, p. 617.
26. Tsarkova, L.A., Zhang, X., Klein, J., and Hadjichristidis, N., *Macromolecules* (in press).
27. Tsarkova, L., Zhang, X., Klein, J., and Hadjichristidis, N., *Macromolecules*, 2002, vol. 35, p. 2817.
28. Shchukin, E.D., Pertsov, A.V., and Amelina, E.A., *Kolloidnaya khimiya* (Colloid Chemistry), Moscow: Vysshaya Shkola, 1992.
29. Sonntag, H. and Strenge, K., *Koagulation und Stabilitat Disperser Systeme*, Berlin: VEB, 1970.
30. Granick, S., *Science* (Washington, DC), 1991, vol. 253, p. 1374.
31. Hu, H.-W. and Granick, S., *Science* (Washington, DC), 1992, vol. 258, p. 1339.
32. Luengo, G., Schmitt, F., Hill, R., and Israelachvili, J., *Macromolecules*, 1997, vol. 30, p. 2482.